JACS
JOURNAL OF THE AMERICAN CHEMICAL SOCIETY

ARTICLE

pubs.acs.org/JACS

Ligand Self-Assembling through Complementary Hydrogen-Bonding in the Coordination Sphere of a Transition Metal Center: The 6-Diphenylphosphanylpyridin-2(1*H*)-one System

Urs Gellrich,[†] Jing Huang,[§] Wolfgang Seiche,[†] Manfred Keller,[†] Markus Meuwly,[*,§] and Bernhard Breit[*,†,‡]

[†]Institut für Organische Chemie und Biochemie and [‡]Freiburg Institute for Advanced Studies, Albert-Ludwigs-Unversität, 79104 Freiburg, Germany

[§]Department of Chemistry, University of Basel, Klingelbergstrasse 80, CH-4056 Basel, Switzerland

Supporting Information

ABSTRACT: Motivated by previous findings which had shown that transition metal catalysts based on the 6-diphenylphosphanylpyridone ligand (6-DPPon, **2**) display properties as a self-assembling bidentate ligand−metal complex, we have performed a thorough study on the bonding situation of this ligand, alone and in the coordination sphere of a late transition metal. Thus, combining a number of spectroscopic methods (UV−vis, IR, NMR, X-ray), we gained insights into the unique structural characteristics of **2**. These experimental studies were corroborated by DFT calculations, which were in all cases in good agreement with the experimental results. The free ligand **2** prefers to exist as the pyridone tautomer **2A** and dimerizes to the pyridone−pyridone dimer **4A** in solution as well as in the crystal state. The corresponding hydroxypyridine tautomer **2B** is energetically slightly disfavored (ca. 0.9 kcal/mol within the up-conformer relevant for metal coordination); hence, hydrogen bond formation within the complex may easily compensate this small energy penalty. Coordination properties of **2** were studied in the coordination sphere of a platinum(II) center. As a model complex, [Cl_2Pt(6-DPPon)$_2$] (**11**) was prepared and investigated. All experimental and theoretical methods used prove the existence of a hydrogen-bonding interligand network in solution as well as in the crystal state of **11** between one 6-DPPon ligand existing as the pyridone tautomer **2A** and the other ligand occupying the complementary hydroxypyridine form **2B**. Dynamic proton NMR allowed to determine the barrier for interligand hydrogen bond breaking and, in combination with theory, enabled us to determine the enthalpic stabilization through hydrogen-bonding to contribute 14−15 kcal/mol.

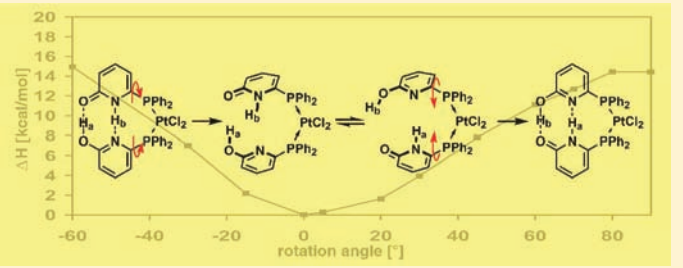

INTRODUCTION

Selectivity control in homogeneous metal complex catalysis is most frequently achieved by crafting the microenvironment of the catalytically active metal center upon binding of appropriate ligand architectures to the metal center. Among the many ligands used, bidentate ligands occupy an important position. Chelation induces a higher binding constant for the metal center and thus provides a higher stability of the resulting metal complexes. Furthermore, the bidentate nature of the ligand reduces the degrees of freedom in the ligand backbone, which in turn decreases the number of competing transition states, resulting in higher reaction selectivity. A prominent example for enantioselectivity control provides β-ketoester reduction with ruthenium(II)−BINAP catalysts (Scheme 1).[1] Another example is the control of regioselectivity for the industrially important rhodium-catalyzed hydroformylation of terminal alkenes, which requires tailor-made bidentate ligands.[2a−c] Among the few ligands known to achieve efficient regiocontrol is the wide bite angle diphosphine XANTPHOS (Scheme 1).[3]

While these bidentate ligands provide unique selectivities, their synthesis can be troublesome and may render the ligands more expensive than the noble metal source. Thus, as an alternative to classical bidentate ligands in which the two donor sites are connected by a covalent connection, we[4a−d] and others[5a−h] recently introduced the concept of monodentate-to-bidentate ligand self-assembly. Thus, mixing monodentate ligands equipped with functional groups capable of complementary hydrogen bonding in the presence of a transition metal salt leads to defined bidentate ligand−metal complexes. The parent system we selected for this approach was the 2-pyridone (**1A**)/2-hydroxypyridine (**1B**) tautomer system. It is known to dimerize in aprotic solvents to form predominantly the symmetrical pyridone dimer **3A** through hydrogen bonding (Scheme 2).[6−9] If D would be a donor atom capable of binding a metal center, a bidentate binding mode would be impossible for dimer **4A** for geometric reasons. Alternatively, formation of the mixed dimer between the

Received: September 24, 2010
Published: December 9, 2010

dx.doi.org/10.1021/ja108639e | *J. Am. Chem. Soc.* 2011, 133, 964–975

Scheme 1. Enantio- and Regioselectivity Control with Selected Metal Catalysts Derived from Bidentate Ligands

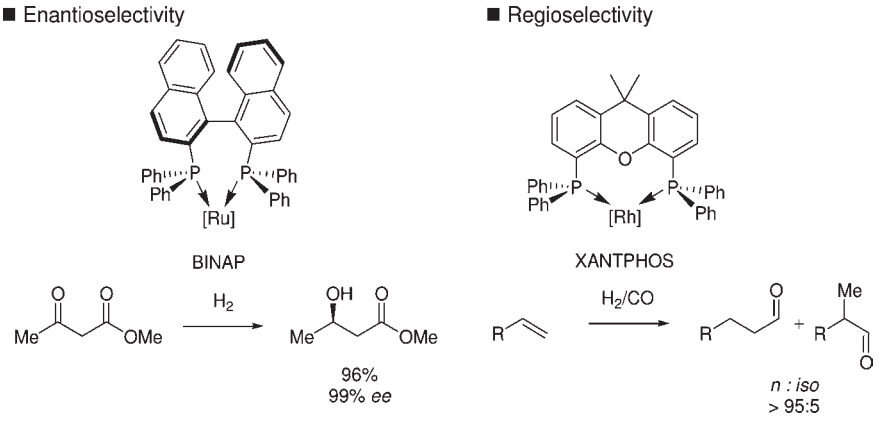

Scheme 2. Self-Assembling of the 6-DPPon Ligand in the Presence of a Transition Metal Center

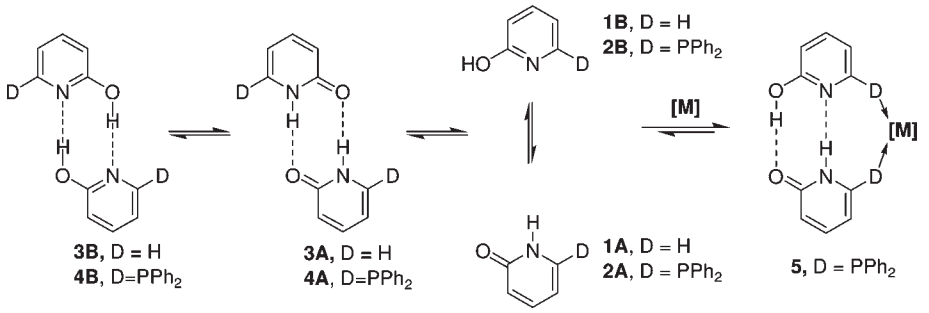

2-pyridone and the 2-hydroxypyridine tautomer would generate a ligand architecture suited for a bidentate binding mode **5**. Although this nonsymmetrical dimerization mode is unusual, recent calculations in the gas phase have shown that it is just 4.8 kcal/mol less favorable (D = H) compared to the commonly observed 2-pyridone dimer.[8] We speculated that if D would be an appropriate donor atom such as a phosphine, the chelation effect exhibited through coordinative binding to a metal center might overcome this energy penalty to provide the bidentate binding mode **5** as shown in Scheme 2. Thus, choosing for D a diphenylphosphanyl function led us to the 6-diphenylphosphanylpyridin-2(1*H*)-one (6-DPPon) system (**2**).[4c,10]

In previous studies we showed that 6-DPPon (**2**) indeed behaves as a bidentate ligand in homogeneous catalysis. We selected the hydroformylation of terminal olefins as a test case since the hydroformylation displays strong chelating effects and only chelating ligands with appropriate large bite angles such as the XANTPHOS system allow for high regioselectivities. Indeed, a rhodium/6-DPPon system furnished a highly active hydroformylation catalyst which displayed high regioselectivity in favor of the linear aldehyde. This catalytic transformation was selected since its regioselectivity is highly sensitive to chelation effects. High regioselectivities in favor of the linear aldehyde were observed with this catalyst in unpolar solvents such as toluene.[4c] However, changing the solvent from toluene to methanol led to significantly reduced levels of regioselectivities which were more typical for a monodentate phosphine ligand (Scheme 3).[11] Hence, these experiments strongly suggest that 6-DPPon forms a bidentate ligand based on complementary hydrogen bonding during the course of the hydroformylation reaction.

Scheme 3. Rhodium-Catalyzed Hydroformylation of 1-Octene: Complementary Behavior of PPh_3 and 2[a]

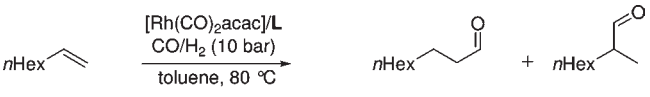

L = PPh_3	72	28
L = 6-DPPon (**2**)	96	4
L = 6-DPPon (**2**) in MeOH	80	20

[a] Reaction conditions: Rh:L:1-octene (1:10:7000), *c*(1-octene) = 1.4 M, 4 h, toluene.

In order to get a deeper insight into the nature and properties of the self-assembling 6-DPPon system, we performed a detailed study on the synthesis of the 6-DPPon ligand (**2**) and its tautomer equilibrium in solution, as well as its coordination behavior in the presence of a platinum(II) center as a model complex for a late transition metal catalyst bearing **2**. Employing UV−vis, IR, and NMR spectroscopy, X-ray crystallography, and DFT methods allowed us to get a detailed insight into the hydrogen-bonding situation and its properties with regard to monodentate to bidentate ligand self-assembly.

■ RESULTS AND DISCUSSION

Synthesis of the 6-DPPon Ligand. The synthesis of **2** commenced from either 2,6-dichloropyridine **6A** or alternatively the dibromo compound **6B**, both commercially available (Scheme 4). One of the halogens was replaced in a nucleophilic aromatic substitution with potassium *tert*-butoxide to furnish the corresponding

Scheme 4. Alternative Preparation of 6-DPPon (2) via a Nucleophilic (Upper Pathway) or Electrophilic Aromatic (Lower Pathway) Displacement

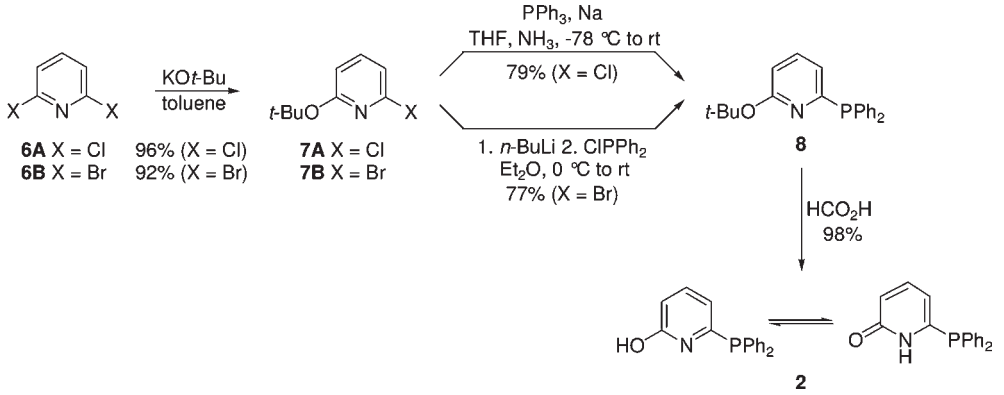

Scheme 5. Preparation of Methyl-Fixed Tautomers 10A (6-DPMePon) and 10B (2-MeODPP)

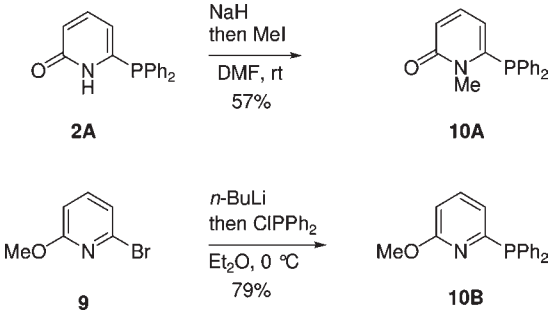

butoxy ethers **7A** and **7B**. Treatment of **7A** with sodium diphenylphosphide, generated under Birch-type conditions from triphenylphosphine, gave the phosphine **8**. This reaction can be run at large scale (50 g). Alternatively, **8** can be obtained from the bromopyridine **7B** upon treatment with *n*-butyllithium at 0 °C in diethyl ether to initiate a bromine−lithium exchange reaction, followed by electrophilic trapping with chlorodiphenylphosphine. Cleavage of the *tert*-butyl ether occurred upon treatment of **8** with formic acid to liberate the 6-DPPon ligand **2**, which was obtained as a colorless solid after recrystallization.

UV−Vis Spectroscopy of 2. Our first goal was to have a deeper look into the equilibrium between the two tautomers of **2**. Hence, we utilized UV−vis spectroscopy, which is a frequently applied method to investigate such tautomeric equilibria. To obtain experimental data for each of the individual tautomers, covalently fixed model substrates **10A** and **10B** were prepared first (Scheme 5). *N*-Methylated and fixed lactam tautomer **10A** was obtained from 6-DPPon (**2**) upon deprotonation with sodium hydride, followed by methylation with methyl iodide. The *O*-methylated system **10B** was obtained starting from bromopyridine **9**. Halogen lithium exchange with *n*-butyllithium and subsequent trapping of the resulting organolithium compound with chlorodiphenylphosphine furnished **10B**.

The UV−vis spectra of 6-DPMePon (**10A**) and 2-MeODPP (**10B**), as well as that of 6-DPPon (**2**), were recorded at a concentration $c = 0.14$ mM in solvents of different polarity (Figure 1). Spectra recorded in dichloromethane showed an absorption maximum for 6-DPMePon (**9A**) at $\lambda = 330$ nm, while the absorption maximum for 2-MeODPP (**10B**) was detected at

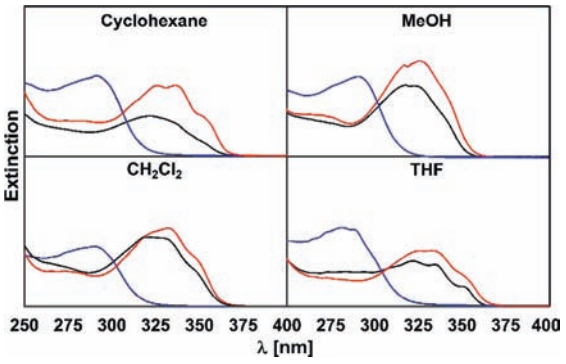

Figure 1. UV−vis spectra of the fixed tautomers **10A** (red) and **10B** (blue) and the free ligand **2** (black) in different solvents. All spectra were recorded at room temperature and a concentration of 0.14 mM.

$\lambda = 290$ nm. Interestingly, the 6-DPPon (**2**) ligand itself showed an absorption maximum at $\lambda = 330$ nm irrespective of the solvent polarity, which shows that the pyridone form **2A** is the prevalent tautomer and thermodynamically favored.

IR Spectroscopy of 6-DPPon (2) in CCl_4 Solution. Typically, NH and OH bonds involved in hydrogen-bonding display stretching vibrations which are shifted to lower wavenumbers compared to those not involved in hydrogen-bonding, and the corresponding absorption bands are significantly broadened.[12] Since the parent 2-pyridone system **1** is known to form symmetric pyridone dimers in aprotic solvents, the appearance of NH···O hydrogen bonds in the IR spectrum of a solution of 6-DPPon (**2**) would suggest the existence of such a dimer **4A** in a similar manner. The IR spectrum of **2** in CCl_4 at $c = 10^{-1}$ M was recorded and is depicted in Figure 2. Additionally, the theoretical IR spectrum for the dimer **4A** and the most stable confomers of both tautomeric forms of the monomer (**2A** and **2B**) were calculated employing DFT methods. The results of experimentally found and calculated absorptions are depicted in Table 1.

According to the calculations, the sharp peak at 1644 cm^{-1} corresponds to the CO vibration of the pyridone form which, in agreement with the results obtained by UV−vis spectroscopy, represents the more stable tautomer of **2**. On the other hand, the extremely broad peak between 2200 and 3200 cm^{-1} corresponds to the N−H···O vibration involved in hydrogen bonding. The origin for the exceptionally broad shape of this peak will be discussed later (*vide infra*). The presence of the N−H···O

dx.doi.org/10.1021/ja108639e |*J. Am. Chem. Soc.* 2011, 133, 964–975

Table 1. Comparison of Characteristic Vibrations (cm^{-1}) Obtained from Experiment and by DFT Calculation of 6-DPPon (2)

		B3LYP/6-31G(d,p)[a]		
	expt	**2A**-down	**2B**-up	**4A**
NH bending vibration	1595/1578	1518 (1580)		1578 (1642)/ 1546 (1609)
OH bending vibration			1580 (1644)	
CO stretching vibration	1644	1715 (1785)		1671 (1738)
CN stretching vibration			1567 (1631)	
N−H···O	2200−3200			3029 (3152)

[a] The vibrations obtained by DFT calculation are scaled by a factor of 0.9611, as proposed by Kacker et al.[13] Unscaled vibrations obtained by means of DFT calculations are shown in parentheses.

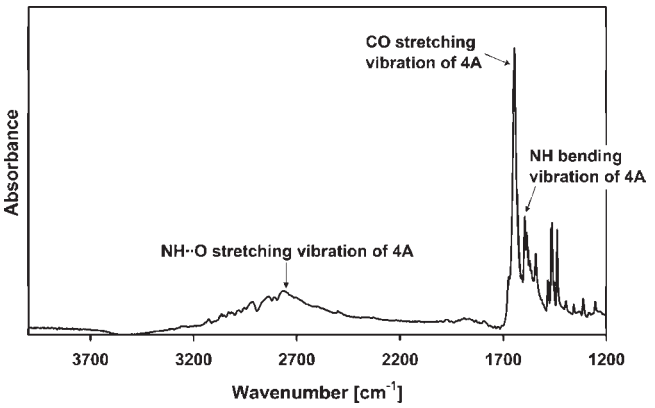

Figure 2. IR spectrum of **2** in CCl_4 ($c = 10^{-1}$ M).

Scheme 6. Association of the Monomeric 6-DPPon Ligand 2A to the Pyridone−Pyridone Dimer 4A

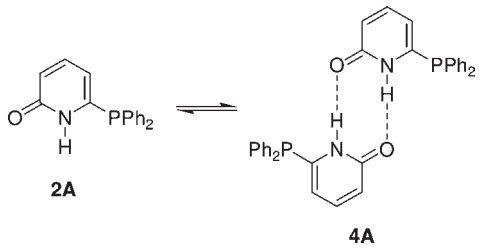

Table 2. Association Constant and ΔG for the Dimerization of 2 Observed by NMR Dilution Experiments and by DFT Calculations

	NMR expt	B3LYP/6-31G(d,p)
K_{ass} (M^{-1})	$(2.31 \pm 0.29) \times 10^4$	2.69×10^4
ΔG (kcal/mol)	-5.95 ± 0.075	-6.05

vibration strongly suggests that a symmetric dimer **4A** of **2** is prevalent in solution under these conditions. Notably, the calculations for **4A** suggest a shift for the CO stretching vibration to lower wavenumbers due to its involvement in hydrogen bonding.

Determination of K_{ass} for the Formation of the Symmetric 6-DPPon Dimer. In order to estimate K_{ass} for the dimerization process of the 6-DPPon monomer (Scheme 6), we performed ^{1}H NMR dilution eperiments.[14] Additionally, we estimated K_{ass} by means of DFT calculations (Table 2).

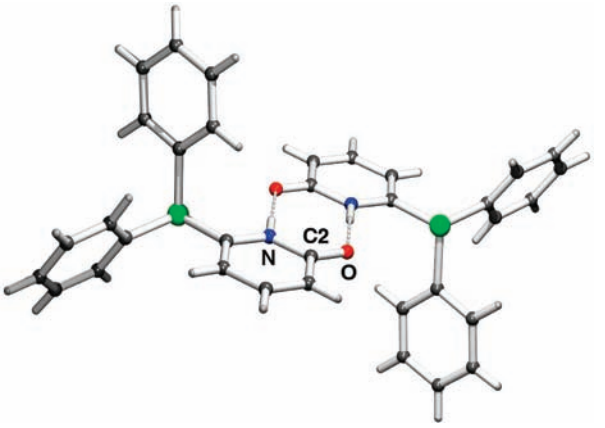

Figure 3. X-ray structure of the symmetric dimer **4A** of 6-DPPon (**2**).

The results obtained from NMR titration as well as those obtained from DFT calculations are in excellent agreement and suggest that dimer formation is thermodynamically favored and, hence, that **4A** is the prevalent species in solution. This result correlates well with former calculations on the pyridone parent system.[8]

Structure of the Symmetric 6-DPPon Dimer. From a saturated solution of **2** in CH_2Cl_2, single crystals could be grown which were suitable for X-ray diffraction analysis. The structure of **2** in the solid state is depicted in Figure 3 and shows the formation of the expected symmetrical pyridone−pyridone dimer **4A**. The formation of the theoretically accessible hydroxypyridine dimer can be excluded on the basis of a comparison of the calculated geometrical data for dimers **4A** and **4B** with those found in the X-ray crystal structure analysis (see Table 3).

The bond lengths show an average difference of 0.05 Å, and the N−H···O angle differs by 2.6°. The only major deviation between theory and experiment is the O···H distance, which differs by 0.17 Å. Here it seems important to point out that the position of the hydrogen atoms in a structure determined by X-ray cannot be detected directly because of the low scattering power of the hydrogen atoms and strongly depends on the mathematical algorithms used to refine the structure. Therefore, the hydrogen positions from the computations are probably more realistic.

Theoretical Analysis of the Conformers and Tautomers of 2. As a next step, we wanted to support our spectroscopic results concerning the tautomerism of **2** by DFT calculations. However, not only is this equilibrium essential for the formation of the proposed hydrogen bonding in the self-assembling process at a metal center, but the heterocycle also has to be in a specific

dx.doi.org/10.1021/ja108639e |J. Am. Chem. Soc. 2011, 133, 964–975

Table 3. Equilibrium Structure of the Dimer of 2 Measured by X-ray and Computed by DFT

		B3LYP/6-31G(d,p)	
	X-ray	**4A**	**4B**
N−H···O (Å)	2.777(1)	2.772	2.737
O···H (Å)	1.89(2)	1.72	1.01
C2−N (Å)	1.377(2)	1.392	1.341
C2−O (Å)	1.250(2)	1.248	1.326
N−H···O (deg)	177.3(2)	179.7	173.4

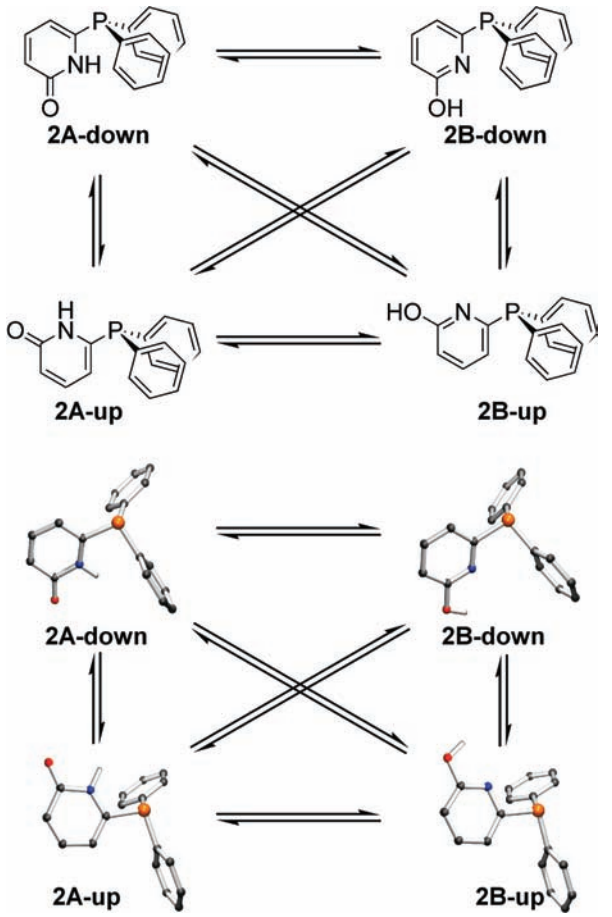

Figure 4. Possible conformers and tautomers of **2** and their DFT optimized structures.

geometrical orientation relative to the PPh_2 group in order to allow for self-assembly to occur. Figure 4 shows the optimized structures of the relevant conformers and tautomers of **2**.

Thus, from the selected conformers, only the "up" conformers allow **2** to form hydrogen bonds to a neighbor ligand system while the phosphorus is bound to the metal center. Furthermore, one ligand must exist in the lactim form **2B** to render hydrogen bonding possible. The energy differences between all conformers and tautomers were determined by DFT calculations. Table 4 shows the energy and Gibbs free enthalpy differences between the conformers and tautomers of **2**.

The calculations clearly show, in agreement with the results obtained by UV−vis spectroscopy, that the pyridone form represents the more stable tautomer. On the other hand, the energy differences are small enough to allow the existence of the disfavored hydroxypyridine form if this energetic penalty could be compensated for by the bond enthalpy of the proposed hydrogen bonds.

Table 4. Relative Energies and Gibbs Free Enthalpy at 298.15 K of the Confomers and Tautomers Shown in Figure 4

	E + ZPE (kcal/mol)[a]	ΔG (kcal/mol)
2A-down	0.0	0.0
2A-up	0.6	0.2
2B-down	2.3	2.2
2B-up	1.5	1.5

[a] E + ZPE = electronic energy + zero point energy.

Scheme 7. Preparation of *cis*-$[Cl_2Pt(6\text{-DPPon})_2]$ Complex 11

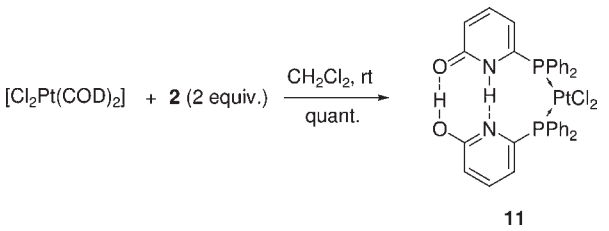

11

Coordination Properties of 6-DPPon: Formation of and Bonding Situation in *cis*-$[Cl_2Pt(6\text{-DPPon})_2]$ (11). Square planar coordination geometries are the most common coordination geometries (among others, including trigonal bipyramidal, octahedral, etc.) passed in catalytic cycles of late transition metal catalysis, and as such it is an ideal model system to explore the coordination behavior of the 6-DPPon ligands. For this reason a platinum(II) salt was selected, since these are known to form square planar coordination geometries upon coordination of two donor ligands, which may exist in either a *cis* or *trans* isomeric form. Reaction of $[Cl_2Pt(COD)]$ with 2 equiv of 6-DPPon ligand **2** furnished quantitatively *cis*-$[Cl_2Pt(6\text{-DPPon})_2]$ (**11**) via displacement of 1,5-cyclooctadiene with the two phosphine donor ligands (Scheme 7).

NMR Spectroscopy of 11. ^{31}P NMR spectroscopy can be used for structural characterization of square planar platinum complexes with two phosphorus ligands, as 30% of the platinum exists as the NMR-active ^{195}Pt isotope ($I = 1/2$), coupling with the ^{31}P atoms. $^1J_{P-Pt}$ coupling constants greater than 3000 Hz are typical for a *cisoid* arrangement of the two phosphane ligands at the platinum center.[15]

The ^{31}P NMR of $[Cl_2Pt(6\text{-DPPon})_2]$ (**11**) is depicted in Figure 5. A $^1J_{P,Pt}$ coupling constant of 3591 Hz was monitored which clearly indicates the two 6-DPPon ligands to be in a *cisoid* arrangement.[16] The *cis* geometry should enable the formation of hydrogen bonds between the two ligands, which could be monitored by ^1H NMR spectroscopy (Figure 6).

Indeed, the ^1H NMR shows two distinct signals in the chemical shift region typically expected for OH or NH bonds involved in hydrogen bonding (δ = 11−13, see Figure 6). Considering the electronegativity of the heteroatoms involved in the hydrogen bonds, the signal at δ = 12.90 could be assigned to the O−H···O proton, whereas the signal at δ = 12.43 corresponds to the absorption of the N−H···N proton. Taking a closer look at this resonance, a poorly resolved doublet can be

dx.doi.org/10.1021/ja108639e | J. Am. Chem. Soc. 2011, 133, 964–975

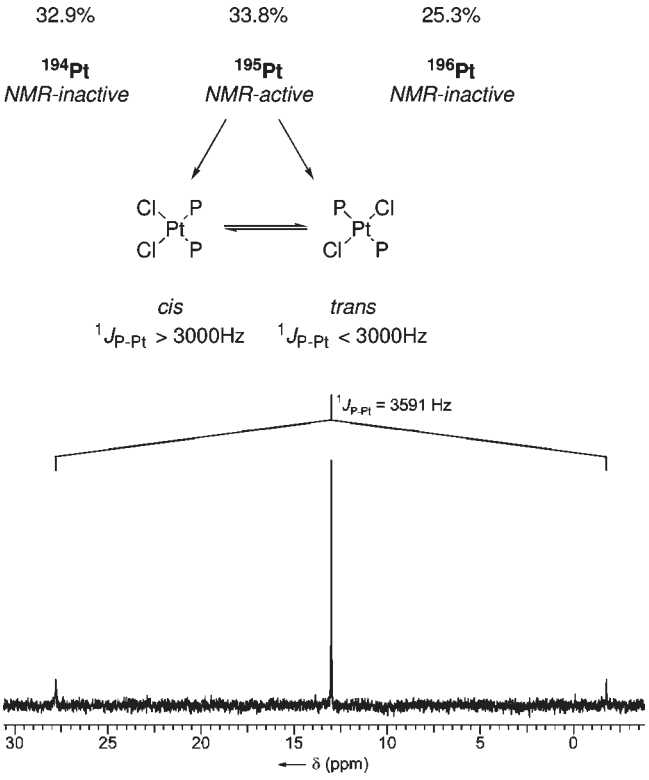

Figure 5. Coupling in complexes of the general type $[Cl_2PtP_2]$ (top) and ^{31}P NMR spectrum for $[Cl_2Pt(6\text{-DPPon})_2]$ (bottom).

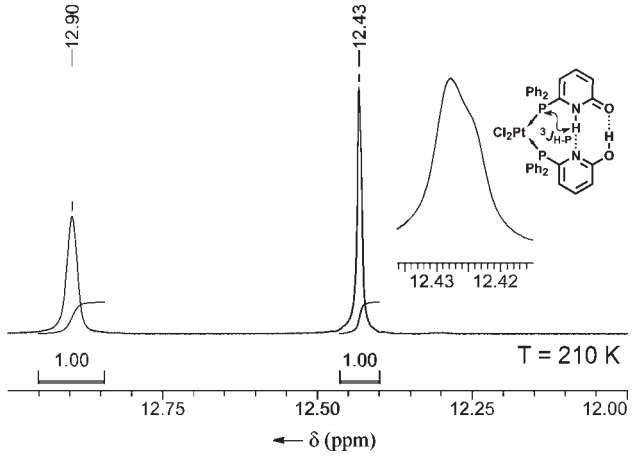

Figure 6. ^1H NMR ($CDCl_3$, 500 MHz, 210 K) spectrum of **11** and a proposed coupling for the signal located at δ = 12.43.

deduced, which results from a $^3J_{H-P}$ coupling with the phosphorus atom in proximity. Dynamic proton NMR spectra show a distinct temperature dependence for the resonances of these protons involved in hydrogen bonding. Thus, coalescence of signals was observed at 325 K, which suggests a highly dynamic and fast tautomerization of the two ligands, rendering the protons on the NMR time scale magnetically equivalent (Figure 7).

Without an explicit line shape analysis, the rate constant was calculated with eq 1.[17]

$$k_c = \frac{\pi\Delta\nu}{\sqrt{2}} = 2.22\Delta\nu \qquad (1)$$

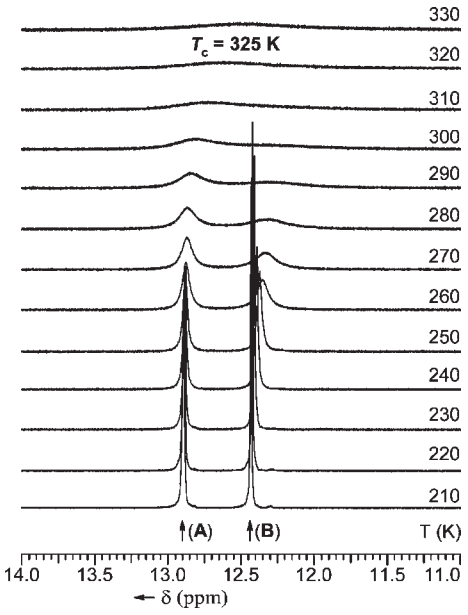

Figure 7. ^1H NMR spectrum of **11** as a function of the temperature.

With a frequency splitting of $\Delta\nu$ = 213.6 Hz at 210 K, a rate constant k_c = 514 s^{-1} was calculated. In the context of Eyring theory, the rate constant is related to the free activation enthalpy.

$$k_c = \frac{k_b T}{h} e^{-\Delta G^{TS}/RT} \qquad (2)$$

In eq 2, k_B represents the Boltzmann constant, h the Planck constant, and R the ideal gas constant. Using this equation, a free activation energy of ΔG^{TS} = 15.1 kcal/mol can be estimated.

The dynamic process which renders the two hydrogen atoms involved in hydrogen bonding equal on the NMR time scale must involve a tautomerization process. However, since within the hydrogen-bonded pseudochelate complex the hydrogen atoms involved in H-bonding are in a fixed orientation, tautomerization is impossible. Thus, in order to tautomerize, the hydrogen-bonding network has to break first, which is achieved by rotating the pyridone and hydroxypyridine nuclei out of plane (step a in Scheme 8). Once the H-bonds are broken, the known pyridone/hydroxypyridine tautomerization can occur (step b in Scheme 8). Renewed hydrogen-bonding (step c in Scheme 8) renders the protons involved in hydrogen bonding magnetically undistinguishable.

For a more quantitative assesssment, the strength of the double-H-bond motif was determined, and the tautomerization reaction was considered in more detail. To computationally characterize the energy required to break the H-bond motif, the two aromatic rings were simultaneously rotated in a disrotatory manner (fixing the two Pt−P−C−H dihedral angles), and the remaining internal degrees of freedom were optimized. The computed energy barrier is 14.6 kcal/mol, which is close to the experimentally determined value of 15.1 kcal/mol. However, it should be pointed out that, experimentally, a free energy (ΔG) is derived from k_c, whereas the present computational approach only reports on the enthalpy change. The N−H and O−H bond lengths are closer to those in the separate 6-DPPon system (1.014 and 0.966 Å) at ϕ = 80°, showing that both hydrogen bonds have been broken (Figure 8).

dx.doi.org/10.1021/ja108639e |J. Am. Chem. Soc. 2011, 133, 964–975

Scheme 8. Process That Renders the Hydrogen Bonds Indistinguishable: (a) Rotation along the C_α−P Bond, (b) Intramolecular Tautomerism, and (c) Rotation Back in Plane and Formation of the Hydrogen Bonds

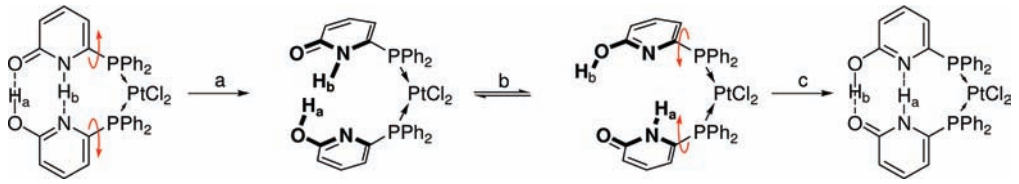

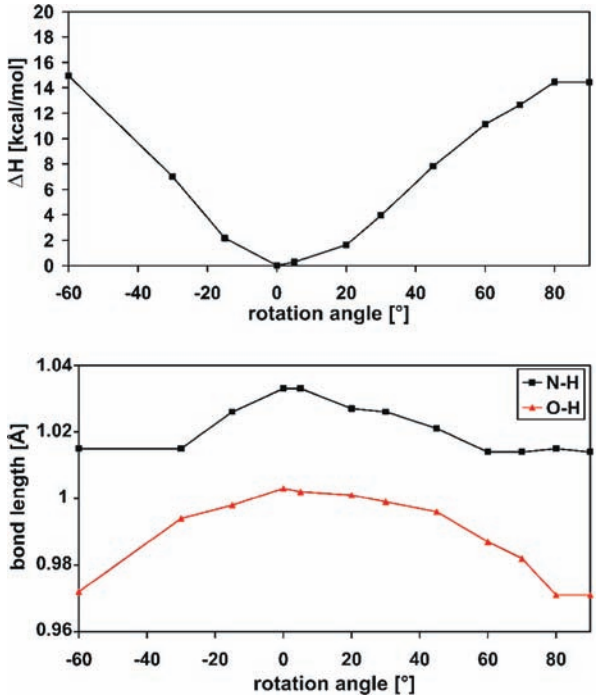

Figure 8. Rotation of pyridone and hydroxypyridine rings from the equilibrium structure. (Top) Change of total energy. (Bottom) Change of N−H and O−H bond lengths.

Tautomerization after hydrogen bond breaking (step b in Scheme 8) for compound **11** was also investigated by using DFT calculations. For this, the barrier for intramolecular OH−N H-transfer for the open conformation (both H-bonds broken) was determined and yields an isomerization barrier of 34 kcal/mol, close to calculations on free 2-pyridone, which found 32 kcal/mol for this process.[18] The work on isolated pyridones has further established that, with varying numbers of water molecules as proton relays, the barrier for enol−keto tautomerization is appreciably affected. It decreases to about 12 and 6 kcal/mol with one and two additional water molecules, respectively. Similar effects are expected for $[Cl_2Pt(6\text{-DPPon})_2]$ (**11**) in contact with water, which cannot be excluded to be present in catalytic amounts in an NMR experiment.

The experimental ΔG^{TS} = 15.1 kcal/mol agrees favorably with the DFT energies for pyridone/hydroxypyridine rotation and concomitant deletion of the double H-bond motif in (**11**), but differs considerably from water-free tautomerization (>30 kcal/mol). The only competitive process is water-assisted tautomerization (around 12 kcal/mol for free 2-pyridone), which, however, requires deletion of the double H-bond motif to occur initially. Thus, the process captured by dynamic proton NMR is most likely the rotatory motion of the pyridone and hydroxypyridine rings and not intramolecular H-transfer. However, to firmly establish this, more elaborate calculations including entropic effects, H-bond dynamics, and explicit solvent will be necessary. For this, molecular dynamics (MD) simulations together with dedicated force fields, such as VALBOND-TRANS,[19] combined with provisions for a realistic treatment of the hydrogen dynamics, such as molecular mechanics with proton transfer, are required.[20] In summary, experimental results from dynamic proton NMR in combination with theoretical DFT calculations show that the hydrogen bonding between the two 6-DPPon ligands within $[Cl_2Pt(6\text{-DPPon})_2]$ (**11**) results in a thermodynamic stabilization of ca. 15 kcal/mol.

Ab initio calculations of the ^{1}H NMR signals of the hydrogen atoms in the N−H−N/O−H−O motifs have also been carried out. In the experimental spectrum, the H signal is found at 12.9/12.43 ppm (T = 210 K) and disappears from the 11−15 ppm range at 320 K. This compares with computed ^{1}H NMR signals of the hydrogen atoms in the N−H···N/O−H···O motifs at 13.33/13.04 ppm (for the equilibrium structure, $\phi = 0°$), where the two H-bonds are formed, and signals at 5.12/8.60 ppm for a structure with broken hydrogen bonds (ϕ = 80°). Thus, the computational results are in qualitative agreement with the experimental data. However, a more accurate assessment of the temperature-dependent ^{1}H NMR spectrum requires conformational sampling by means of finite-temperature molecular dynamics (MD) simulations together with dedicated force fields (see above).

UV−Vis Spectroscopy. In addition to NMR spectroscopy, UV−vis spectroscopy should be capable to provide further evidence for the formation of the hydrogen-bonding interligand network within $[Cl_2Pt(6\text{-DPPon})_2]$ (**11**). Since we showed that the isolated 6-DPPon ligand **2** alone energetically prefers to exist as the pyridone tautomer **2A**, detection of the hydroxypyridine tautomer **2B** in the UV−vis spectrum of $[Cl_2Pt(6\text{-DPPon})_2]$ (**11**) would be further evidence for the existence of the interligand hydrogen bonding. Since the coordination of the ligands to the platinum center might change the UV spectroscopy of the pyridone/hydroxypyridine chromophores, we prepared the platinum complexes with the "fixed tautomer" models **10A** and **10B** first (Scheme 9), following the same protocol as for the preparation of the 6-DPPon complex **11**.

While **12B** was formed as the *cis* isomer only, **12A** was obtained as a *cis*/*trans* mixture of isomers in the ratio of 45/55, as determined by ^{31}P NMR spectroscopy and analysis of the $^1J_{P-Pt}$ coupling constants. Figure 9 displays the UV−vis spectra of the complexes **12B**, **12A**, and **11** in CH_2Cl_2 solution (c = 2.5 μM).

Indeed, the UV−vis spectrum of **11** appears as the superposition of the spectra obtained for fixed tautomer complexes **12A** and **12B**. Hence, the fact that both tautomeric forms **2A** and **2B** of the 6-DPPon ligand are present in the complex gives

dx.doi.org/10.1021/ja108639e |*J. Am. Chem. Soc.* 2011, 133, 964–975

Scheme 9. Synthesis of the Pt Complexes Bearing the Fixed Tautomers of 2

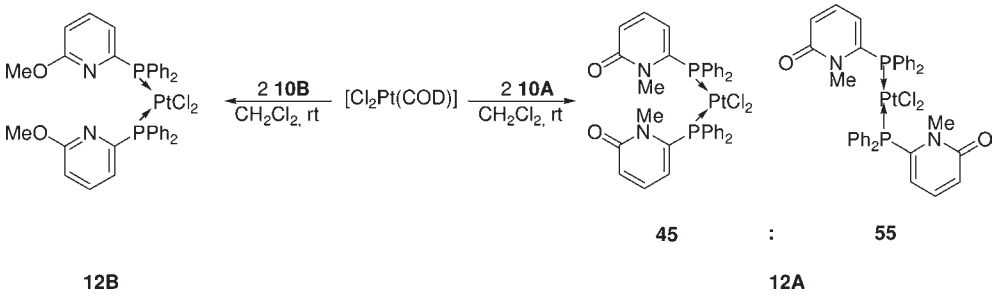

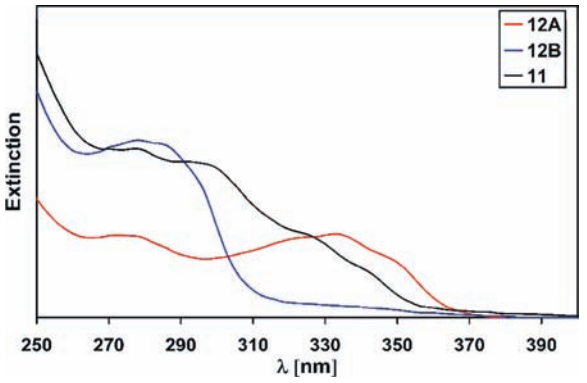

Figure 9. UV−vis spectra of **11** (black), **12A** (red), and **12B** (blue). The spectra were recorded in CH_2Cl_2 at room temperature and a concentration of 2.5 μM.

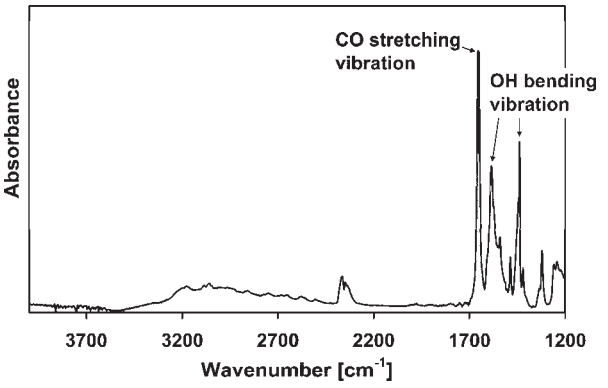

Figure 10. IR spectrum of complex **11** in CCl_4 at room temperature and a concentration of 10^{-3} M.

another hint that both tautomeric forms are present in $[Cl_2Pt(6\text{-}DPPon)_2]$ (**11**). The only possible explanation for the existence of the energetically unfavorable hydroxypyridine isomer is its involvement in hydrogen bonding with the complementary pyridone tautomer, which more than compensates the energetic cost for tautomerization through hydrogen bonding.

IR Spectroscopy of 11. For further insight into the bonding situation within $[Cl_2Pt(6\text{-}DPPon)_2]$ (**11**), we chose IR spectroscopy, which should allow us to detect the presence of hydrogen bonding as well as whether one of the ligands is present in its hydroxypyridine tautomeric form **2B**. The IR spectrum of **11** was recorded as a solution in CCl_4 ($c = 10^{-3}$ M) and is depicted in Figure 10. Additionally, DFT calculations of **11** were carried out to allow assignment of vibrational bands (see Table 5).

The vibration at 1653 cm^{-1} (Figure 10) can be identifed as the CO stretching vibration of **2A**. Furthermore, the absorptions at 1584 cm^{-1} (Figure 10) and 1440 cm^{-1} could be identified as the OH rocking vibrations of the hydroxypyridine tautomer (Figure 10).

Taking into account the situation for the free 6-DPPon ligand **2**, in which the pyridone form is thermodynamically more stable and prevalent, the presence of a hydroxypyridine form within complex **11** must be due to the fact that hydrogen bonds are formed between the two 6-DPPon ligands within complex **11** in solution. Thus, the bond enthalpy of the hydrogen bonds enables the transition of the pyridone into the energetically less favored hydroxypyridine form.[20] By comparing the spectrum of free **2** with the recorded IR spectrum of **11** (Figure 11), it is obvious that the vibrations at 1584 cm^{-1} and 1440 cm^{-1}, are only present in the metal complex, indicating the formation of a heterodimeric species.

The unusually broad peak between 2500 and 3500 cm^{-1} shown in Figure 10 is assigned to the hydrogen bonds (NH···N and OH···O) in the complex. The vibrational transitions associated with hydrogen motion in such strong hydrogen bonds are very sensitive to the chemical environment and the corresponding infrared signatures usually exhibit a diffuse character.[22a,b] We computed the IR spectrum for the equilibrium structure of the $[Cl_2Pt(6\text{-}DPPon)]$ complex **11** and also for a series of structures for which both, the N−H and O−H bonds were simultaneously elongated by 0.01, 0.03, and 0.05 Å. The harmonic frequencies of the H-stretching modes in the NH···N and OH···O motifs are highlighted by red lines in Figure 12, and clearly link the observed broad band between 2500 cm^{-1} and 3500 cm^{-1} to motion along the hydrogen bond.

Table 5. Comparison of Characteristic Vibrations (cm^{-1}) Obtained from Experiment and by DFT Calculation of $[Cl_2Pt(6\text{-}DPPon)_2]$ (11)

	expt	B3LYP/6-31G(d,p)[a]
CO stretching vibration	1653	1668 (1735)
OH rocking vibration	1584/1440	1554 (1616)/1451 (1510)
N−H···N, O−H··O	2500−3500	2500−3500[b]

[a] Both scaled and unscaled frequencies (in parentheses) are shown, as in Table 1. [b] See Figure 10 and discussion.

Experimental and Computed Structure for the $[Cl_2Pt(6\text{-}DPPon)_2]$. A final proof for the existence of interligand hydrogen bonding within $[Cl_2Pt(6\text{-}DPPon)_2]$ (**11**) came from an X-ray crystal structure analysis of suitable single crystals obtained from a saturated solution of **11** in dichloromethane. The molecular structure of **11** in the crystal state is depicted in Figure 13. It clearly shows two 6-DPPon ligands coordinated to the platinum center in a *cis* fashion. The two phosphine ligands

dx.doi.org/10.1021/ja108639e |J. Am. Chem. Soc. 2011, 133, 964–975

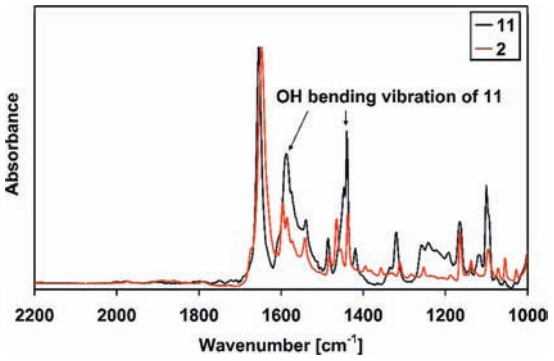

Figure 11. Direct comparison between the IR spectra of **2** and **11**.

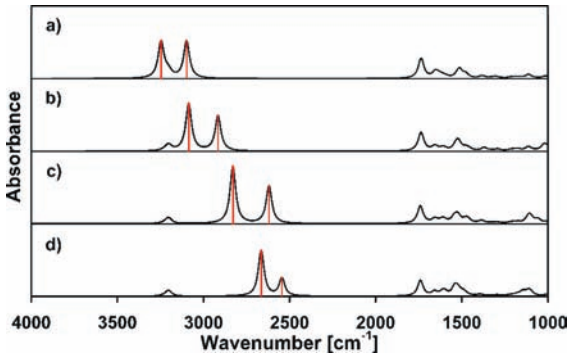

Figure 12. Computed IR spectrum for a) equilibrium structures b) N−H and O−H bond lengths increased by 0.01 Å; c) N−H and O−H bond lengths increased by 0.03 Å; d) N−H and O−H bond lengths increased by 0.05 Å, and with all other degrees of freedom optimized. The red lines indicate the frequencies of hydrogen bond stretching as assigned from the normal modes. The N−H/O-H stretching frequencies are found to be very sensitive to the geometry of the H-bonds.

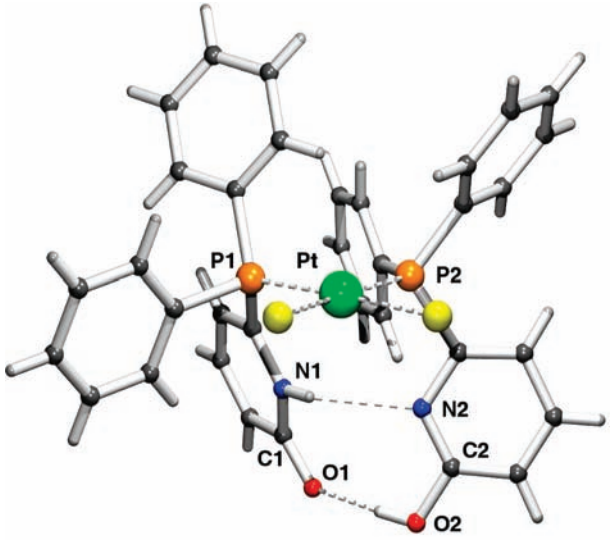

Figure 13. Crystal structure of $[Cl_2Pt(6\text{-DPPon})_2]$ complex **11**. The hydrogen bonds are represented as dashed lines.

are crystallographically distinct. One of them exists in the lactam form **2A** and the other in the lactim form **2B**, which is obvious from the different bond lengths within the corresponding heterocycles (pyridone vs hydroxypyridine). The X-ray structure

Table 6. Equilibrium Structure of the $[Cl_2Pt(6\text{-DPPon})_2]$ Complex Measured by X-ray and Computed by DFT

	X-ray	B3LYP/6-31G(d,p)/LANL2DZ
Pt−P1 (Å)	2.2563(6)	2.313
Pt−P2 (Å)	2.2364(6)	2.306
P1−Pt−P2 (deg)	97.58(2)	106.0
N1−H (Å)	0.84(3)	1.033
N2···H (Å)	2.40(3)	1.990
N1···N2 (Å)	3.071(3)	2.966
N1···H···N2 (deg)	137(3)	156.3
O2−H2 (Å)	0.86(4)	1.003
O1···H2 (Å)	1.85(4)	1.632
O1···O2 (Å)	2.683(3)	2.631
O2···H−O1 (deg)	164(4)	173.3

finally suggests the formation of hydrogen bonds between the two tautomeric complementary 6-DPPon ligands based on the bond distances between O1−O2 and N1−N2, respectively (see Table 6). A comparison of the experimental data with those obtained from a DFT calculation is in good agreement (Table 6). For example, the Pt−P bond lengths differ by only 0.06 Å, and the P−Pt−P natural bite angles differ by 9°. The distances between the pyridone ring and the hydroxypyridine ring are also comparable: the difference in N···N distances is 0.1 Å, while that of O···O distances is 0.05 Å. However, in the DFT structure, the N−H and O−H bond lengths are elongated to 1.033 and 1.003 Å, respectively, and the N···H···N and O···H···O motifs are almost linear. This is a strong indication for hydrogen bonding between the 6-DPPon ligands, which is not seen in the X-ray structure since the corresponding electron density is asymmetrical and not centered at the position of the nucleus. As mentioned before, in general, locating hydrogen atoms in X-ray crystallography is difficult because of their low scattering power and librational effect, and the refined structure depends on the computational algorithms used.

CONCLUSIONS

Motivated by previous findings, which had shown that transition metal catalysts based on the 6-diphenylphosphanylpyridone ligand (6-DPPon, **2**) display unique properties and suggested that 6-DPPon behaves as a monodentate-to-bidentate self-assembling ligand, we herein performed a thorough study on the bonding situation of this ligand, alone and in the coordination sphere of a late transition metal. Thus, combining a number of spectroscopic methods (UV−vis, IR, NMR, X-ray) corroborated by DFT calculations, insights into the unique structural characteristics of 6-DPPon (**2**) were gained. The free ligand **2** prefers to exist as the pyridone tautomer **2A** and dimerizes to the pyridone−pyridone dimer **4A** in solution as well as in the crystal state. The corresponding hydroxypyridine tautomer **2B** is slightly disfavored energetically (ca. 0.9 kcal/mol within the up-conformer relevant for metal coordination). Hence, hydrogen bond formation within the complex is expected to easily compensate this small energy penalty. This was confirmed experimentally by studying the coordination properties of **2** within the model complex $[Cl_2Pt(6\text{-DPPon})_2]$ (**11**). All experimental and theoretical methods used are consistent with the existence of a hydrogen-bonding interligand network in solution as well as in the crystal state of **11** between one 6-DPPon ligand existing as the

pyridone tautomer **2A** and the other ligand occupying the complementary hydroxypyridine form **2B**. Dynamic proton NMR allowed us to determine the barrier for interligand hydrogen bond breaking and, in combination with theory, led to an estimate for the enthalpic stabilization through hydrogen bonding of 15 kcal/mol. Hence, a theoretical understanding of the ground-state structural features of this self-assembling ligand **2** is now available and ready to be used to further explore its unique properties as a ligand in homogeneous catalysis.

METHODS

Experimental Methods. All reagents were obtained commercially unless otherwise noted. Reactions were performed using oven-dried glassware under an atmosphere of argon. Air- and moisture-sensitive liquids and solutions were transferred via syringe. Organic solutions were concentrated under reduced pressure (ca. 20 mbar) by rotary evaporation. Toluene was distilled from sodium, dichlormethane and MeOH were distilled from CaH_2, THF was distilled from potassium, and diethyl ether was refluxed over a potassium−sodium alloy using benzophenone ketyl radical as indicator and distilled prior to use. All solvents were stored under an argon atmosphere. Chromatographic purification of products was accomplished using flash chromatography on Macherey-Nagel silica gel 60 (230−400 mesh). Nuclear magnetic resonance spectra were acquired on a Varian Mercury spectrometer (300, 121.5, and 75.5 MHz for ^{1}H, ^{31}P, and ^{13}C, respectively) and on a Bruker AMX 400 (400.1 and 100.6 MHz for ^{1}H and ^{13}C, respectively) and are referenced internally according to residual protio solvent signals. Data for ^{1}H and ^{31}P NMR are recorded as follows: chemical shift (δ, ppm), multiplicity (s, singlet; bs, broad singlet; d, doublet; t, triplet; pt, pseudotriplet; q, quartet; quint, quintet; m, multiplet), coupling constant (Hz), integration. Data for ^{13}C NMR are reported in terms of chemical shift (δ, ppm). **9** was prepared from commercially available **6B** according to the literature known procedure.[23]

*Synthesis of 2-tert-Butoxy-6-chloropyridine (**7A**).* To a solution of 2,6-dichloropyridine (**6A**) (10.0 g, 67.6 mmol, 1.00 equiv) in toluene (150 mL) was added potassium *tert*-butoxide (9.10 g, 81.1 mmol, 1.20 equiv). After heating for 6 h to 80 °C, the suspension was filtered over Celite and the solvent removed under reduced pressure. Distillation (bp = 200 °C, 10^{-2} mbar) yielded 11.98 g (64.53 mmol, 96%) of 2-*tert*-butoxy-6-chloropyridine (**7A**) as a colorless liquid.

^{1}H NMR (400.1 MHz, $CDCl_3$, ppm) = 7.43 (t, J = 7.7 Hz, 1H), 6.81 (d, J = 7.3 Hz, 1H), 6.53 (d, J = 8.2 Hz, 1H), 1.58 (s, 9H). ^{13}C NMR (100.6 MHz, $CDCl_3$, ppm) = 163.3, 147.7, 140.2, 115.7, 111.3, 80.9, 28.6. CHN analysis calcd: C, 58.23; H, 6.52; N, 7.54. Found: C, 58.27; H, 6.65; N, 7.48.

*Synthesis of 2-tert-Butoxy-6-bromopyridine (**7B**).* To a solution of 2,6-dibromopyridine (**6B**) (9.48 g, 40.0 mmol, 1.00 equiv) in toluene (150 mL) was added potassium *tert*-butoxide, and the suspension was stirred for 4 h at 80 °C. The reaction mixture was filtered over Celite and the solvent removed under reduced pressure. Distillation (bp = 120 °C, oil pump vacuum) yielded 8.50 g (36.7 mmol, 92%) of the desired product as a colorless liquid.

^{1}H NMR (400.1 MHz, $CDCl_3$, ppm) = 7.34 (m, 1H), 6.98 (d, J = 7.3 Hz, 1H), 6.57 (d, J = 8.2 Hz, 1H), 1.59 (s, 9H). ^{13}C NMR (100.6 MHz, $CDCl_3$, ppm) = 163.1, 140.1, 137.7, 119.5, 111.5, 80.9, 28.5.

*Synthesis of 2-tert-Butoxy-6-diphenylphosphanylpyridine (**8**).* To liquid ammonia (ca. 500 mL) at −78 °C was added sodium (5.40 g, 235 mmol, 2.03 equiv) over 10 min. The dark blue solution was treated portionwise first with triphenylphosphine (30.4 g, 116 mmol, 1.00 equiv) and then, after stirring for 2 h at −78 °C, with 2-*tert*-butoxy-6-chloropyridine (**7A**, 21.5 g, 116 mmol, 1.00 equiv). After addition of 175 mL of tetrahydrofuran, the ammonia was allowed to evaporate overnight. The residue was quenched with 200 mL of water (distilled), extracted three times with 150 mL portions of diethyl ether, and dried over Na_2SO_4. Evaporation of the solvent *in vacuo* and recrystallization of the residual oil from methanol yielded 31.0 g (92.4 mmol, 79%) of 2-*tert*-butoxy-6-diphenylphosphanylpyridine (**8**) as a white solid.

Alternatively, 2-*tert*-butoxy-6-bromopyridine (**7B**, 100 mg, 0.43 mmol, 1.00 equiv) was dissolved in Et_2O (3 mL) and cooled to 0 °C. After addition of *n*-BuLi (0.28 mL, 0.43 mmol, 1.56 M in hexane), the solution was stirred for 60 min at 0 °C. Chlorodiphenylphosphine was added, and the reaction mixture was stirred at room temperature for an additional 60 min. Water (1 mL) was added and the solvent removed under reduced pressure. Purification of the residue by column chromatography over silica gel (CH_2Cl_2) yielded 125 mg (0.34 mmol, 77%) of 2-*tert*-butoxy-6-diphenylphosphanylpyridine (**8**) as a white solid.

mp = 77 °C. ^{1}H NMR (400.1 MHz, $CDCl_3$, ppm) = 7.51−7.44 (m, 4H), 7.11−7.04 (m, 6H), 6.91 (ddd, J = 8.3, 7.3, 2.8 Hz, 1H), 6.75 (dd, J = 7.3, 2.8 Hz, 1H), 6.45 (d, J = 8.3 Hz, 1H), 1.41 (s, 9H). ^{13}C NMR (100.6 MHz, $CDCl_3$, ppm) = 164.1, 160.5, 138.0, 137.6, 134.7, 128.9, 128.7, 121.4, 112.2, 79.6, 28.5. ^{31}P NMR (121.5 MHz, $CDCl_3$, ppm) = −1.7. CHN analysis calcd: C, 75.21; H, 6.61; N, 4.18. Found: C, 74.98; H, 6.57; N, 4.09.

*Synthesis of 6-Diphenylphosphanyl-1H-pyridin-2-one (6-DPPon, **2**).* 2-*tert*-Butoxy-6-diphenylphosphanylpyridine (**8**, 9.7 g, 28.9 mmol) was dissolved in concentrated formic acid (100 mL) saturated with argon. After stirring for 30 min at room temperature, the solution was diluted with water (distilled, 120 mL). The precipitate was collected by filtration, washed with 30 mL of aqueous formic acid (2:1, v/v), and dried. 6-Diphenylphosphanyl-1*H*-pyridin-2-one (**2**) was obtained as a white solid (5.6 g, 20.05 mmol, 69%). The combined aqueous formic acid solutions were concentrated *in vacuo*, and the residue was recrystallized from acetone. This yielded another 1.8 g (6.45 mmol, 22%) of 6-diphenylphosphanyl-1*H*-pyridin-2-one (**2**).

mp = 187 °C. ^{1}H NMR (400.1 MHz, $CDCl_3$, ppm) = 9.29 (br s, 1H), 7.45−7.25 (m, 11H), 6.51 (d, J = 9.0 Hz, 1H), 6.20 (t, J = 6.3 Hz, 1H). ^{13}C NMR (100.6 MHz, $CDCl_3$, ppm) = 163.8, 146.6, 140.5, 133.9, 132.6, 130.2, 129.3, 120.7, 114.0. ^{31}P NMR (121.5 MHz, $CDCl_3$, ppm) = −8.5. CHN analysis calcd: C, 73.11; H, 5.05; N, 5.02. Found: C, 72.97; H, 5.18; N, 4.73.

*Synthesis of 6-Diphenylphosphanyl-1-methylpyridin-2-one (6-DPMePon, **10A**).* To a solution of 6-diphenylphosphanylpyridine-2(1*H*)-one (**2**, 500 mg, 1.79 mmol, 1.00 equiv) in DMF (8 mL) was added sodium hydride (46.0 mg, 1.91 mmol, 1.07 equiv) in one portion. After gas evolution ceased, the solution was cooled to 0 °C. Methyl iodide (255 mg, 1.80 mmol, 1.00 equiv) was added, and the reaction mixture was stirred for 30 min at room temperature. After addition of water (20 mL), the organic layer was separated and washed with Et_2O. After drying with $MgSO_4$, the solvent was removed under reduced pressure, and the residue was purified by column chromatography over silica gel (CH_2Cl_2:PE 1:1 to CH_2Cl_2 to CH_2Cl_2:EE 1:1), yielding 300 mg (1.02 mmol, 57%) of the desired product as a colorless liquid.

mp = 159 °C. ^{1}H NMR (400.1 MHz, $CDCl_3$, ppm) = 7.37−7.46 (m, 6H), 7.29−7.35 (m, 4H), 7.14 (ddd, J = 8.8 Hz, J = 7.1 Hz, J = 1.5 Hz, 1H), 6.54 (d, J = 9.0 Hz, 1H), 5.62 (d, J = 6.9 Hz, 1H), 3.58 (s, 3H). ^{13}C NMR (100.6 MHz, $CDCl_3$, ppm) = 164.2, 150.6, 137.8, 134.3, 132.9, 130.2, 129.2, 119.8, 113.3, 33.8. ^{31}P NMR (121.5 MHz, $CDCl_3$, ppm) = −11.1. CHN analysis calcd: C, 73.71; H, 5.50; N, 4.78. Found: C, 73.42; H, 5.73; N, 4.75.

*Synthesis of 2-Methoxy-6-diphenylphosphinopyridine (2-MeODPP, **10B**).* To a solution of 2-methoxy-6-bromopyridine (**8**, 855 mg, 4.55 mmol, 1.00 equiv) in Et_2O (25 mL) was added *n*-BuLi (3.25 mL, 4.55 mmol, 1.40 M in hexane, 1.00 equiv) dropwise at 0 °C. The solution was stirred for 1 h at 0 °C, and chlorodiphenylphosphane (0.82 mL, 1.00 g, 4.55 mmol, 1.00 equiv) was added at this temperature. The reaction mixture was allowed to warm to room temperature and stirred for 5 h. The reaction mixture was diluted with CH_2Cl_2 (50 mL) and

filtered through silica gel. The solvent was removed under reduced pressure, and the residue was purified by column chromatography over silica gel (PE/CH_2Cl_2 2:1 to 1:1). Distillation (bp = 160 °C, 10^{-2} mbar) yielded 1.10 g (3.60 mmol, 79%) of the desired product as a colorless solid.

mp = 59 °C. ^{1}H NMR (400.1 MHz, $CDCl_3$, ppm) = 7.40−7.48 (m, 5H), 7.33−7.38 (m, 6H), 6.77 (dd, J = 7.2 Hz, J = 2.2 Hz, 1H), 6.63 (d, J = 8.3 Hz, 1H), 3.83 (s, 3H). ^{13}C NMR (100.6 MHz, $CDCl_3$, ppm) = 163.7, 160.2, 138.1, 136.8, 134.3, 128.9, 128.4, 121.8, 110.0, 53.5. ^{31}P NMR (121.5 MHz, $CDCl_3$, ppm) = −2.6. CHN analysis calcd: C, 73.71; H, 5.50; N, 4.78. Found: C, 73.54; H, 5.50; N, 4.72.

*Synthesis of [Cl_2Pt(6-diphenylphosphanyl-1H-pyridin-2-one)$_2$] (**11**).* To a solution of *cis*-[Cl2Pt(COD)] (68.4 mg, 182 μmol, 1.00 equiv) in CH_2Cl_2 (2.5 mL) was added 6-diphenylphosphanyl-1*H*-pyridin-2-one (**2**, 102.0 mg, 366 μmol, 2.00 equiv) at room temperature. The solution was diluted with CH_2Cl_2 (2.5 mL) and stirred for 2 h at room temperature. The solvent was removed under reduced pressure and the resulting solid washed two times with pentane (2 × 5 mL). The product was obtained as a colorless solid (117 mg, 182 μmol, 100%).

^{1}H NMR (400 MHz, $CDCl_3$, ppm) = 12.90 (bs, 1H), 12.43 (bs, 1H), 7.50−7.60 (m, 8H), 7.30−7.38 (m, 6H), 7.22 (pt, J = 6.8 Hz, 8H), 6.73 (d, J = 8.8 Hz, 2H), 6.48 (pt, J = 6.4 Hz, 2H). ^{13}C NMR (100.6 MHz, $CDCl_3$, ppm) = 164.6, 143.8, 140.2, 134.8, 131.5, 128.3, 128.1, 118.3, 117.8. ^{31}P NMR (121.5 MHz, $CDCl_3$, ppm) = 13.0 ($^1J_{P-Pt}$ = 3591.4 Hz).

Suitable crystals for X-ray analysis were grown from a solution of 20 mg of **11** in CH_2Cl_2 (absolute, 1 mL) at room temperature.

UV−Vis Spectroscopy. Solvents used for UV−vis spectroscopy were purified as described in the Experimental Methods section. The spectra of the fixed tautomers **10A** and **10B** and the free ligand **2** were recorded on a Perkin Elmer 15 spectrometer at room temperature and a concentration of 0.14 mM. The spectra of the platinum complexes **11**, **12A**, and **12B** were recorded using a Perkin Elmer Lambda 950 spectrometer at a concentration of 2.5 μM in CH_2Cl_2 at room temperature. The complexes [Cl_2Pt(6-diphenylphosphanyl-1-methyl-pyridine-2-one)$_2$] (**12A**) and [Cl_2Pt(2-methoxy-6-diphenylphosphanylpyridine)$_2$] (**12B**) were prepared by stirring [Cl_2Pt(COD)] (10.9 mg, 0.02 mmol, 1.00 equiv) with 6-diphenylphosphino-1-methylpyridin-2-one (**10A**) and 2-methoxy-6-diphenylphosphinopyridine (**10B**) (10.0 mg, 0.03 mmol, 2.00 equiv) in CH_2Cl_2 (2.5 mL) at room temperature for 2 h, respectively. The solvent was removed under reduced pressure, and the residue was diluted to a concentration of 2.5 μM. An aliquot was taken from the solution to confirm the formation of the desired complex by means of ^{31}P NMR.

cis-[Cl_2Pt(6-diphenylphosphanyl-1-methylpyridin-2-one)$_2$] (**12A**): ^{31}P NMR (121.5 MHz, $CDCl_3$, ppm) = 12.8 ($^1J_{P-Pt}$ = 3626.8 Hz).

trans-[Cl_2Pt(6-diphenylphosphanyl-1-methylpyridin-2-one)$_2$]: ^{31}P NMR (121.5 MHz, $CDCl_3$, ppm) = 17.3 ($^1J_{P-Pt}$ = 2686.4 Hz).

cis-[Cl_2Pt(2-methoxy-6-diphenylphosphanylpyridine)$_2$] (**12B**): ^{31}P NMR (121.5 MHz, $CDCl_3$, ppm) = 13.8 ($^1J_{P-Pt}$ = 3655.4 Hz).

IR Spectroscopy. Solvents used for IR spectroscopy were purified as described in the Experimental Methods section. All spectra were recorded using a ReactIR 45 m FT-IR spectrometer. In a typical experiment the IR flask, equipped with a magnetic stirrer, was filled with CCl_4 (4 mL) under an inert atmosphere of argon at room temperature. After 16 min, solvent spectra were recorded and subtracted, and a solution of **11** (2.1 mg, 0.0025 mmol) or **2** (140 mg, 0.5 mmol), dissolved in CCl_4 (1 mL), was added. The solution was stirred for 1 h 45 min, and a spectrum was recorded every 60 s.

Computational Methods. All structures are fully optimized by using Density Functional Theory (DFT) with the B3LYP functional.[24] All calculations were carried out with the all-electron 6-31G(d,p) basis set[25] for C, H, N, O, and P atoms and an LANL2DZ effective core potential[26] for Pt and Cl atoms. Infrared (IR) and NMR spectra are calculated at the same level of theory from a harmonic vibrational analysis and the GIAO gauge method,[27,28] respectively. All electronic structure calculations were carried out using the Gaussian03 suite of programs[29] with the grid=ultrafine option.

■ ASSOCIATED CONTENT

Supporting Information. Energies and Cartesian coordinates of optimized **2A**, **2B**, **4A**, **4B**, and **11**; ^{31}P NMR spectra of **12A** and **12B**; complete ref 29; details of the NMR dilution experiment; X-ray crystallographic data, in CIF format, for **4A** and **11**. This material is available free of charge via the Internet at http://pubs.acs.org.

■ AUTHOR INFORMATION

Corresponding Author
bernhard.breit@chemie.uni-freiburg.de; m.meuwly@unibas.ch

■ ACKNOWLEDGMENT

Funding of both groups via the IRTG 1038 "Catalysts and Catalytic Reaction for Organic Synthesis" from DFG and the Swiss National Science Foundation is acknowledged. The work in Freiburg was further supported by the Fonds of the Chemical Industry (Ph.D. fellowship to U.G.) and the Alfred-Krupp Award (to B.B.). The Freiburg group is indebted to the companies BASF and Umicore for gifts of precious metal salts. The work in Basel is supported by the Swiss National Science Foundation under Grant No. 200021-117810 (to M.M.).

■ REFERENCES

(1) Miyashita, A.; Yasuda, A.; Takaya, H.; Toriumi, K.; Ito, T.; Souchi, T.; Noyori, R. *J. Am. Chem. Soc.* **1980,** *102*, 7932.

(2) (a) Devon, T. J.; Philips, G. W.; Puckette, T. A.; Stavinoha, J. L.; Vanderbilt, J. J. U.S. Patent 4 694 109,1987. (b) Billig, E.; Abatjoglou, A. G.; Bryant, D. R. U.S. Patent 4 769 498, 1988. (c) Cunny, G. D.; Buchwald, S. L. *J. Am. Chem. Soc.* **1993,** *114*, 5535.

(3) Kranenburg, M.; v. d. Burgt, Y. E. M.; Kamer, P. C. J.; v. Leeuwen, P. W. N. M.; Goubitz, K.; Fraanje, J. *Organometallics* **1995,** *14*, 3081.

(4) (a) Breit, B. *Angew. Chem.* **2005,** *117*, 6976. (b) *Angew. Chem., Int. Ed.* **2005,** *44*, 6816. (c) Breit, B.; Seiche, W. *J. Am. Chem. Soc.* **2003,** *125*, 6608. (d) *Pure Appl. Chem.* **2006,** *78*, 249.

(5) (a) For a review on alternative approaches to self-assembled ligand/catalyst libraries, see ref 4b. See also: (b) Takacs, J. M.; Reddy, D. S.; Moteki, S. A.; Wu, D.; Palencia, H. *J. Am. Chem. Soc.* **2004,** *126*, 4494. (c) Slagt, V. F.; Röder, M.; Kamer, P. C. J.; van Leeuwen, P. W. N. M.; Reek, J. N. H. *J. Am. Chem. Soc.* **2004,** *126*, 4056. (d) Slagt, V. F.; van Leeuwen, P. W. N. M.; Reek, J. N. H. *Angew. Chem., Int. Ed.* **2003,** *42*, 5619. (e) Slagt, V. F.; van Leeuwen, P. W. N. M.; Reek, J. N. H. *Chem. Commun.* **2003,** 2474. (f) Ding, K.; Du, H.; Yuan, Y.; Long, J. *Chem.—Eur. J.* **2004,** *10*, 2872. (g) Sandee, A. J.; v. d. Burg, A. M.; Reek, J. N. H. *Chem. Commun.* **2007,** 864. (h) Gulyás, H.; Benet-Buchholz, J.; Escudero-Adan, E. C.; Freixaa, Z.; van Leeuwen, P. W. N. M. *Chem.—Eur. J.* **2007,** *13*, 3424.

(6) Beak, P. *Acc. Chem. Res.* **1977,** *10*, 186.

(7) Fischer, C. B.; Polborn, K.; Steiniger, H.; Zipse, H. *Z. Naturforsch.* **2004,** *59b*, 1121.

(8) Chou, P.-T.; Wei, C.-Y.; Hung, F.-T. *J. Phys. Chem. B* **1997,** *101*, 9119.

(9) For a review on complementary hydrogen-bonding motifs for the self-assembly of supramolecular architectures see: Lehn, J.-M.; Krische, M. J. *Struct. Bonding (Berlin)* **2000,** *94*, 3.

(10) Akazome, M.; Suzuki, S.; Shimizu, Y.; Henmi, K.; Ogura, K. *J. Org. Chem.* **2000,** *65*, 6917.

(11) Breit, B.; Krische, M. J. *Metal catalyzed reductive C-C bond formation*; Springer: Berlin-Heidelberg, 2007.

(12) Günzler, H.; Gremlich, H.-U. *IR-Spektroskopie*; Wiley-VCH: Weinheim, 2003.
(13) Irikura, K. K.; Johnson, R. D., III; Kacker, R. N. *J. Phys. Chem. A* **2005,** *109*, 8430.
(14) For details see the Supporting Information.
(15) (a) Pregosin, P. S.; Kunz, R. W. *31P and 13C NMR of Transition Metal Phosphine Complexes in NMR Basic Principles and Progress*; Springer: Heidelberg, 1979. (b) Alt, H. G.; Baumgartner, R.; Brune, H. A. *Chem. Ber.* **1986,** *119*, 1694.
(16) The fact that the two P atoms in the platinum complex display a singlet in the ^{31}P NMR spectrum means that they are magnetically equivalent at the NMR time scale. This can be explained by our calculations which identified a transition state for proton transfer by DFT. The activation energy was calculated to be 7.9 kcal/mol, which corresponds to a rate for tautomerization of 0.011 ns^{-1}. This is much faster than the microsecond (NMR) time scale, which renders the P atom connected to the pyridone ring and the P atom connected to the hydroxypyridine system indistinguishable in the ^{31}P NMR experiment.
(17) Friebolin, H. *Ein- und zweidimensionale NMR-Spektroskopie*; Wiley-VCH: Weinheim, 1999.
(18) Tsuchida, N.; Yamabe, S. *J. Phys. Chem. A* **2005,** *109*, 1974.
(19) Tubert-Brohman, I.; Schmid, M.; Meuwly, M. *J. Chem. Theory Comput.* **2009,** *5*, 530.
(20) Lammers, S.; Lutz, S.; Meuwly, M. *J. Comput. Chem.* **2008,** *29*, 1048.
(21) Shuklov, I. A.; Dubrovina, N. V.; Barsch, E.; Ludwig, R.; Michalik, D.; Börner, A. *Chem. Commun.* **2009,** 1535.
(22) (a) Meuwly, M.; Müller, A.; Leutwyler, S. *Phys. Chem. Chem. Phys.* **2003,** *5*, 2663. (b) Roscioli, J. R.; McCunn, L. R.; Johnson, M. A. *Science* **2007,** *316*, 249.
(23) Zhang, W.; Luo, Z.; Chen, C. H.-T.; Curran, D. P. *J. Am. Chem. Soc.* **2002,** *124*, 10443.
(24) Becke, A. D. *J. Chem. Phys.* **1993,** *98*, 5648.
(25) Hehre, W. J.; Ditchfield, R.; Pople, J. A. *J. Chem. Phys.* **1972,** *56*, 2257.
(26) Hay, P. J.; Wadt, W. R. *J. Chem. Phys.* **1985,** *82*, 270.
(27) Ditchfield, R. *Mol. Phys.* **1974,** *27*, 789.
(28) Wolinski, K.; Hilton, J. F.; Pulay, P. *J. Am. Chem. Soc.* **1990,** *112*, 8251.
(29) Frisch, M. J.; et al. *Gaussian 03*, Revision C.02; Gaussian, Inc.: Wallingford, CT, 2004.